

doi: 10.18720/MCE.74.8

Modeling of indentation and slip of wedge punch

Моделирование внедрения и сдвига штампа клиновидной формы

A.S. Semenov,
S.G. Semenov,
B.E. Melnikov,
*Peter the Great St. Petersburg Polytechnic
University, St. Petersburg, Russia*
V.S. Tikhonov,
Weatherford, Moscow Russia

*Канд. физ.-мат. наук, доцент А.С. Семенов,
инженер С.Г. Семенов,
д-р техн. наук, проф. Б.Е. Мельников,
Санкт-Петербургский политехнический
университет Петра Великого,
г. Санкт-Петербург, Россия*
**канд. техн. наук, заведующий сектором
В.С. Тихонов,**
Weatherford, Москва, Россия

Key words: modeling; experiment; elasticity; plasticity; slip; drillpipe; indentation; punch; contact; finite element method

Ключевые слова: моделирование; эксперимент, упругость; пластичность; клиновый захват; бурильная труба; внедрение; штамп; контакт; метод конечных элементов

Abstract. To determine the load-carrying capacity of the drillpipe slip, it is necessary to calculate the drag force on the surface between the pipe and the slip. To improve such capacity, the grip surface is provided with teeth that can indent into the pipe body. As a result, the friction force on the contact surface is supplemented with the drag force generated by plastic shear strain of the pipe body. The paper presents an analytic dependence of the indentation force of an ideal (untruncated) and non-ideal (truncated) wedge punch that models tooth operation on the indentation depth and friction factor on the punch lateral face both for shallow (with prevailing elastic strain of the gripped body) and deep indentation (with prevailing plastic strain). Multiple computational experiments were performed to identify parameters of the proposed formula. Such computations were complemented with determination of the punch drag force dependence on the indentation depth during punch shearing. The developed model was verified by experimental studies of punch indentation and slip as well as indentation and drag force measurements. The obtained results proved the high level of accuracy of the analytical indentation force model. The outcome of drag force determination experiments was further used to calculate the slip load-carrying capacity.

Аннотация. При определении несущей способности клинового захвата бурильных труб возникает проблема расчета силы контактного сопротивления на поверхности раздела захвата и удерживаемой им конструкции. Для повышения надежности поверхность захватывающего устройства снабжается зубцами, которые могут внедряться в тело конструкции. В результате наряду с силой трения на контактной поверхности будет дополнительно действовать сила сопротивления, вызванная пластической деформацией тела при сдвиге. В статье предложена аналитическая зависимость для силы внедрения штампа идеальной (неусеченной) и неидеальной (усеченной) клиновидной формы, моделирующей работу зубца, в зависимости от глубины внедрения и коэффициента трения на боковой поверхности штампа как при неглубоком (с преимущественно упругим деформированием захватываемого тела), так и при глубоком внедрении (с преимущественно пластическим деформированием). Для идентификации параметров предложенной формулы были выполнены многовариантные вычислительные эксперименты. Расчет дополнялся определением зависимости силы сопротивления штампа при сдвиге от глубины внедрения. С целью верификации разработанной модели были проведены экспериментальные исследования процессов внедрения и сдвига штампа с измерением сил внедрения и сопротивления. Полученные результаты подтвердили высокую точность аналитической модели для силы внедрения. Результаты эксперимента с определением силы сопротивления были в дальнейшем использованы для расчета удерживающей силы клинового захвата.

Introduction

Slips, slip elevators, spiders, etc. have been widely used as oilfield service tools to hold drillstrings, drill collars and casings acting as a wedge [1] (Fig. 1). A pipe in a slip with a conical bearing surface is subjected to compound loads comprised of axial tensile, compression and bending stresses. To increase the holding force, the bearing surface of the gripping device is provided with teeth that can indent into the pipe body. This generates additional drag force on the contact surface resulting from plastic strain of the pipe surface as it shears relative to the slip that supplements the friction force.

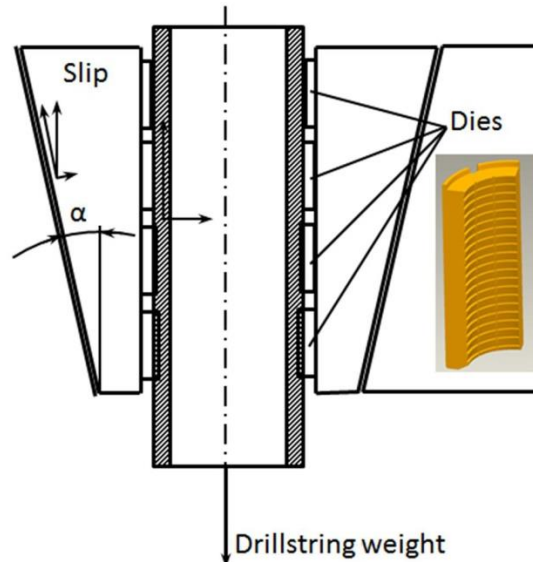


Figure 1. Slip scheme

The Reinhold-Spiri equation [2] accounting for the maximum breaking stress limit being equivalent (von Mises) stress is used in drilling mechanics to determine the holding force. Pipe failures in slips during deepwater drilling in the 1990s and full-scale experiments demonstrated that in some cases the Reinhold-Spiri equation could provide a non-conservative estimation [3]. This results from pipe strength reduction as its surface is damaged by teeth.

An accurate model of contact interaction of the pipe contact surface with the gripping device equipped with teeth of various forms is required for better understanding of causes of pipe breaking in a slip. Such model is based on a single tooth model where such tooth can be considered as a wedge punch: ideal (untruncated) or non-ideal (truncated).

Finite element (FE) modeling of the indentation and scratch processes of a wedge-shaped indenter are considered in [4-8], while experimental investigations are discussed in [9-11, 6, 5]. However, a universal analytical description, which takes into account the wedge geometry, process staging and friction, which oriented to practice, was not proposed.

The purpose of this study is to develop a unified universal model of deep and shallow indentation and shift of an ideal and non-ideal wedge-shape punch, taking into account the dependence of force on the depth of the indented tooth, its geometry and friction on the lateral surface. To achieve the goal, analytical and experimental studies along with numerical simulations are carried out.

The analytic dependences for the indentation force from the depth of wedge teeth indentation into the pipe body are developed for the most common shapes of teeth used in oilfield service tools. In case of shallow (elastic) truncated wedge indentation, it is offered to use known solutions of the linear elastic problem of rectangular shaped punch pressure on half space. The dependence of indentation force on indentation depth and friction factor on the lateral wedge face in case of deep (plastic) indentation is more complex. Parameters of such dependence were identified by multiple FE method computations, where the wedge drag force dependence on the indentation depth during its shearing was additionally calculated. The calculations used both the simplest rigid ideally plastic models [12-14] and elastic-plastic models with nonlinear hardening [15-17].

The developed model is verified by multiple experimental studies of indentation and shift with indentation, breakout and drag force measurements. The obtained results proved the high level of accuracy of the proposed models and can be used to calculate the force of pipe holding in a slip.

Experimental Data

The experimental setup used for wedge punch (single slip tooth) indentation and shear testing was comprised of Instron 8801 multipurpose test system with additional accessories (Fig. 2) to create force normal to the main force generated by the test system. Instron 8801 is a servohydraulic testing system with a maximum load capacity of 100kN and stroke of ~ 80mm. The force measurement accuracy is $\pm 0.5\%$ of indicated load (load cell capacity 1:100), crosshead position measurement accuracy is $\pm 1\ \mu\text{m}$. Accessories (Fig. 2) include tooth holder 1, lower table 2 with above installed U-shaped frame 3. Pipe segment 4 is installed on lower table 2 on special mandrel 5. The mandrel is installed on roller guides 6 to reduce the measurement error. Besides, movement in the perpendicular plane is limited by four adjustable rollers 7 to exclude any movement normal to the applied shear force. Shear force (marked with a blue arrow in Fig. 2) is generated by jack 8 actuated by a manual pump, force is measured with load cell 9 with an accuracy of $\pm 200\ \text{N}$. Shear is measured with LVDT transducer 10 with an accuracy of $\pm 1\ \mu\text{m}$ fixed on frame 3.

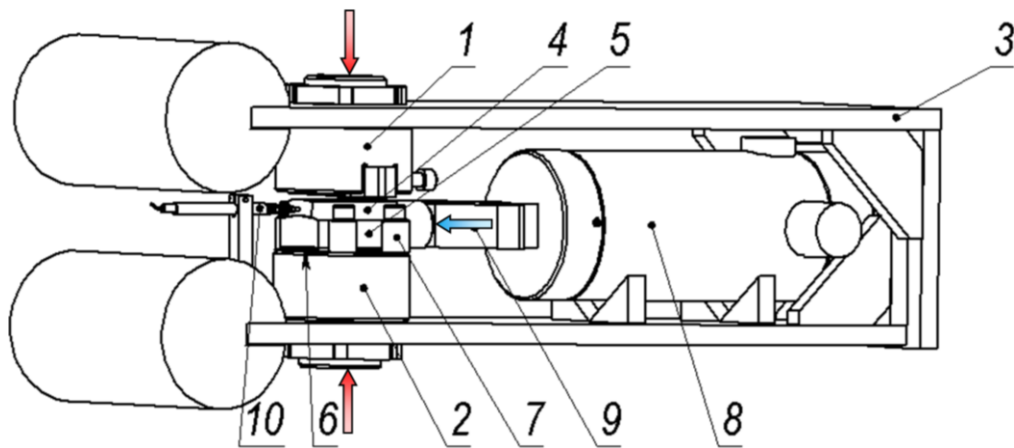


Figure 2. Single tooth test setup

The test program was as follows:

- The tooth was indented to a set depth with the multipurpose test system with simultaneous recording of the indentation diagram using the developed software;
- While the constant indentation depth was maintained, the pipe segment was sheared in relation to the tooth using the jack driven by a manual pump with simultaneous recording of the indentation force and shear force vs. shear diagram using the developed software.

Figure 3 presents the results of single tooth indentation into the pipe segment for as-received and ground surfaces and three depths ($\sim 150\ \mu\text{m}$, $\sim 350\ \mu\text{m}$ and $\sim 750\ \mu\text{m}$). The diagrams were plotted by averaging of three tests with further correction for the system compliance. Based on the above diagrams, the indentation curves for corroded surfaces feature a sufficiently large statistical variability while ground surface curves practically do not demonstrate such variability.

It was established that indentation depth during testing should be measured excluding as many compliant elements as possible. Optimally, noncontact measurement methods should be used that measure the distance between the tooth and the pipe segment.

Figure 4 presents shear curves for various depths and surface conditions. Such curves demonstrate sensitivity both to the indentation depth and surface condition. The appearance of specimens after the shear tests is shown in Figure 5.

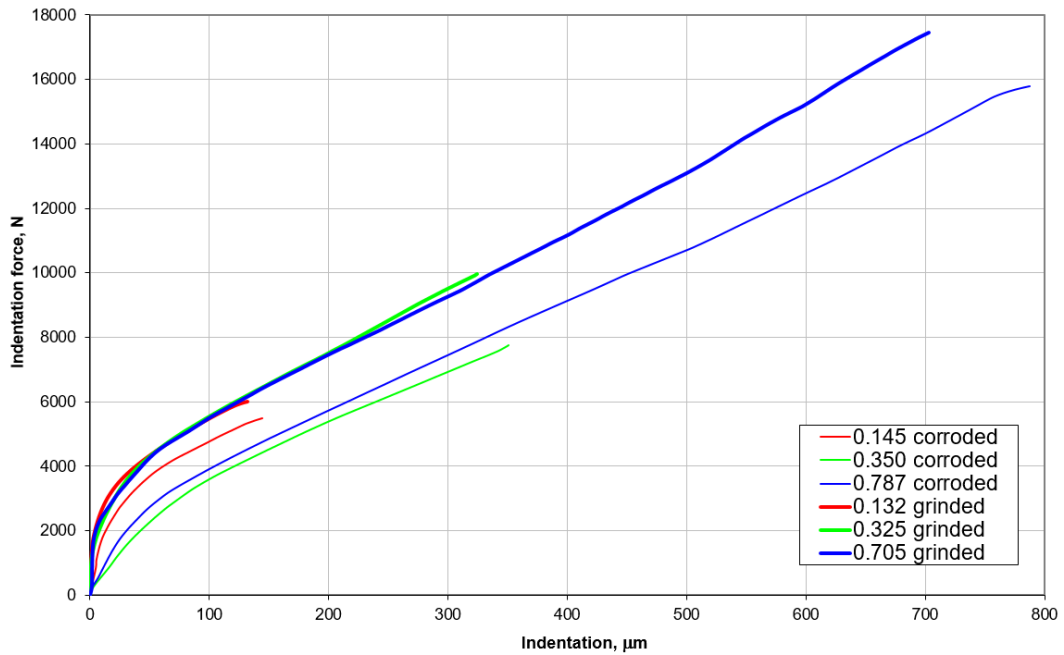


Figure 3. Sample experimental indentation curves

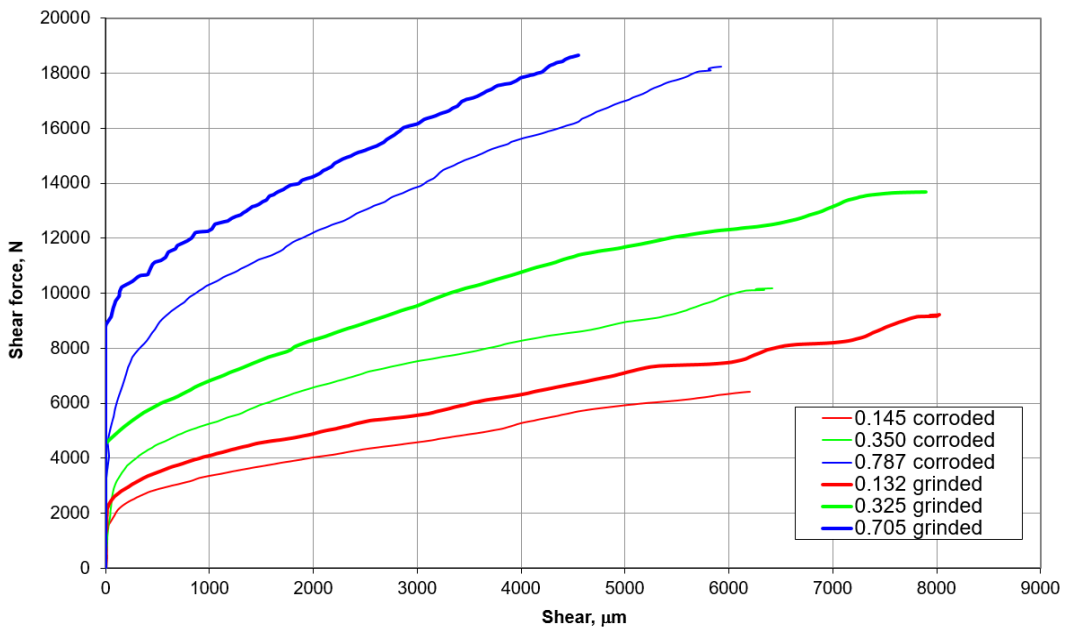


Figure 4. Sample experimental shear curves



Figure 5. Appearance of specimens after indentation with further shear tests. Initial indentation depth: a) 150 μm , b) 350 μm , c) 750 μm

An interpolation surface (Fig. 6) was plotted for ground specimens based on the test results, which represented shear force dependence on the indentation depth and shear.

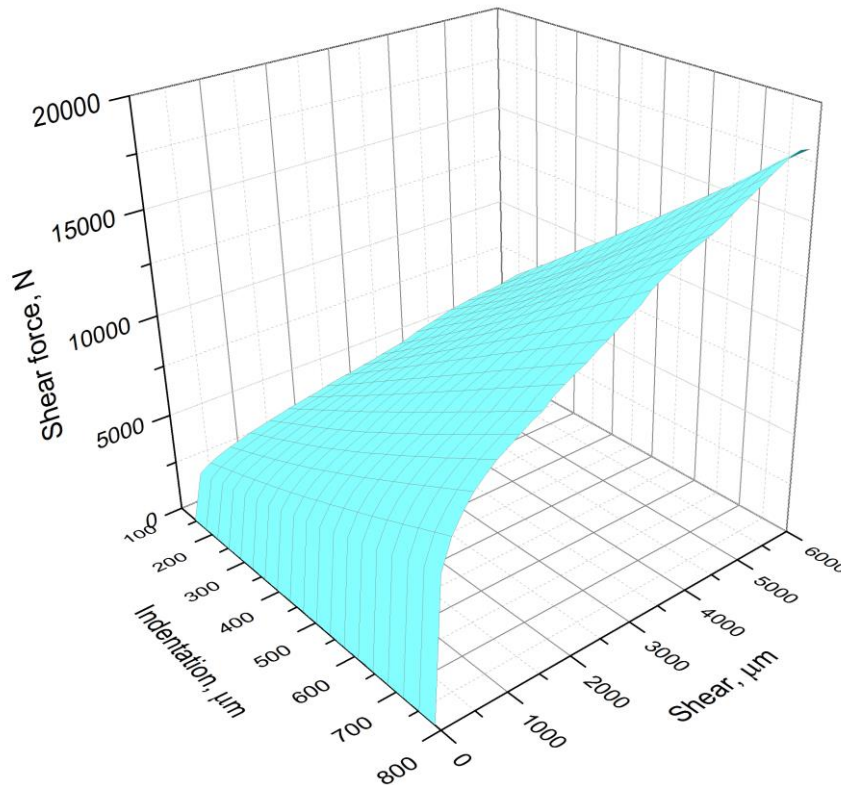


Figure 6. Interpolation surface of shear force dependence on indentation and shear

The resulting dent profiles were measured at the indentation depth of $150\mu\text{m}$ (ground surface) (Fig. 7). Depth was measured with MIG measuring head in the grooved section (accuracy $\pm 1\mu\text{m}$) and a dial gauge in the “crest” section (accuracy $\pm 10\mu\text{m}$). Positioning in the shear direction was ensured by the lathe carriage with an accuracy of $\pm 50\mu\text{m}$.

A section with newly formed smooth surface (about 2mm in the shear direction) and a ruptured section can be distinguished on all the tested specimens. The correct description of the ruptured section requires utilization of fracture mechanics methods [18, 19].

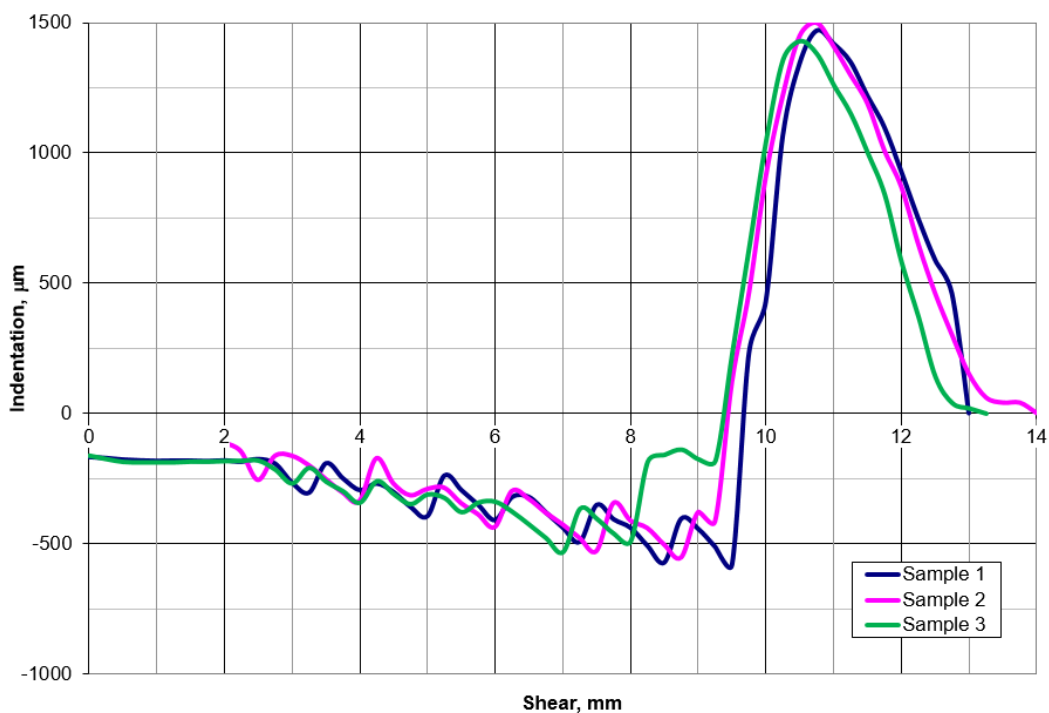


Figure 7. Dent profiles for the initial indentation depth of $150\mu\text{m}$

Approximation of indentation curves of ideal (untruncated) and non-ideal (truncated) wedge punch

Mathematical formulation of indentation model

The representative experimental indentation curve (plotted by averaging of multiple tests) of a symmetric wedge punch with a rectangular flat base (Fig. 8) takes the form of a monotonic increasing dependence of force on indentation depth $F = F(h)$, tending to an oblique asymptote not passing through the origin of coordinates.

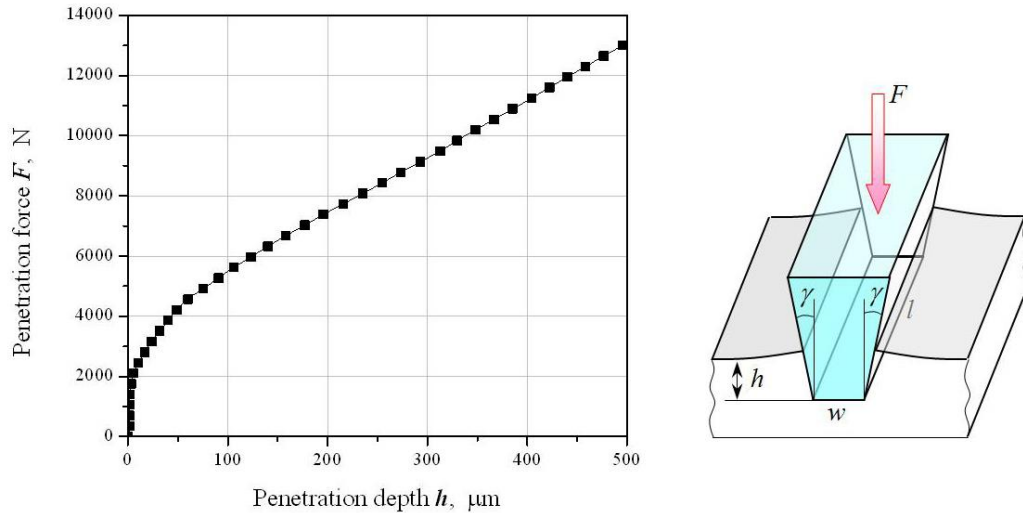


Figure 8. Representative experimental indentation curve (left) of a wedge punch with a rectangular flat base (right) ($w=381\mu\text{m}$, $l=4.826\mu\text{m}$, $\gamma=30^\circ$)

To approximate indentation curves of ideal and non-ideal (flat base) wedge punches $F = F(h)$, this paper proposes to use the following equation:

$$F = (k_p h + F_0) \left(1 - e^{-\frac{k_e h}{F_0}} \right), \quad (1)$$

which at $h \rightarrow \infty$ asymptotically tends to the straight line:

$$F = k_p h + F_0, \quad (2)$$

and at $h \rightarrow 0$ to the straight line:

$$F = k_e h. \quad (3)$$

Equation (1) uses three parameters: k_e, k_p, F_0 , which characterize the initial and final slopes of the indentation curve and the height of asymptote intersection with Y-axis (Fig. 9):

$$\begin{aligned} k_e &= \left. \frac{dF}{dh} \right|_{h \rightarrow 0} \\ k_p &= \left. \frac{dF}{dh} \right|_{h \rightarrow \infty} \\ F_0 &= [F(h) - k_p h]_{h \rightarrow \infty} \end{aligned} \quad (4)$$

The validity of equalities (4) can be easily verified using equation for the derivative of $F(h)$ function (1):

$$\frac{dF}{dh} = k_p \left(1 - e^{-\frac{k_e h}{F_0}} \right) + \left(k_p h + F_0 \right) \frac{k_e}{F_0} e^{-\frac{k_e h}{F_0}}. \quad (5)$$

The choice of the exponent function used to describe the nonlinear indentation curve segment is proved by the calculation data, which does not preclude searching of any alternatives.

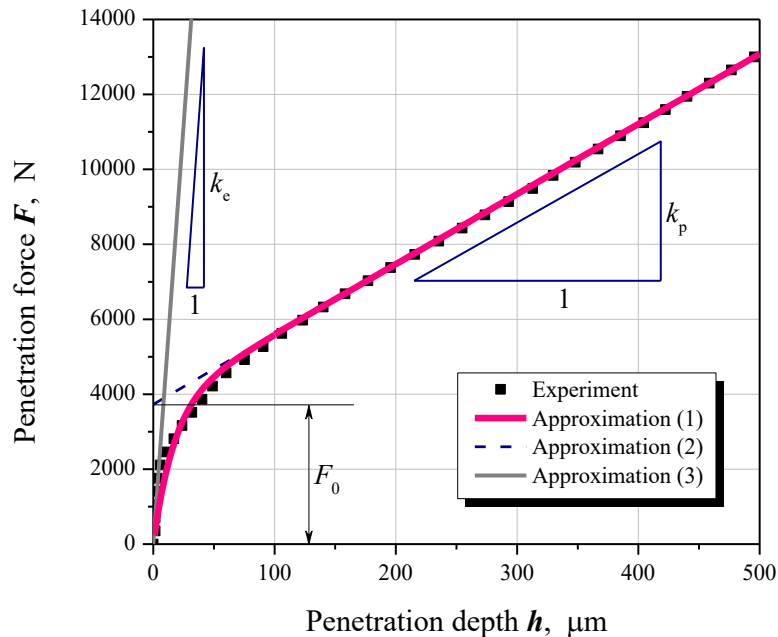


Figure 9. Approximation (1) of the indentation curve of a wedge punch with a rectangular flat base and geometric interpretation of its parameters

To analyze processes of indentation of *non-ideal* (truncated) wedges to considerable depths $h > w/7$, where w is the truncated wedge base width, linear approximation (2) can be used instead of (1), which differs from (1) by less than 0.1% for typical values of used wedge parameters. When indentation processes of *ideal* ($w = 0$) wedges are analyzed, there is no pressure contribution in the area perpendicular to the action of force ($F_0 = 0$) and it would be reasonable to use the simplified equation

$$F = k_p h. \quad (6)$$

Approximation in the form of Eq. (1) using three parameters k_e, k_p, F_0 can be justified by the ability to estimate the latter based on the known analytical solutions of contact problems in the context of the theory of elasticity (for k_e) and theory of plasticity (for k_p, F_0). It should be noted that, in the general case, parameters k_e, k_p, F_0 admit dependence on the wedge geometry and mechanical properties of the indenting and indented material. Analytical solutions help define the above dependences concretely.

Elastic and plastic analytic solutions

At the *initial* stage ($h \rightarrow 0$) of indentation of a wedge punch with a flat base, solution of the *linear elastic problem* of punch pressure with a rectangular base on half space [20, 21] can be used:

$$F = \frac{E}{1 - \nu^2} \frac{\sqrt{wl}}{m} h, \quad (7)$$

where E is Young's modulus, ν is Poisson's ratio, w is the truncated wedge base width, l is the truncated wedge base length, m is the parameter determined as the ratio of the base sides (if $l/w = 10$ $m = 0.71$, Fig. 10). Eq. (7) was derived by generalization of the solution of the Boussinesq problem on the action of a normal concentrated force on the surface of elastic half-space. It should be noted that solution (7) was derived based on the assumptions of infinitesimal mechanics, where small strains are assumed and the difference between the actual and reference configurations are neglected. In this case, the form of the wedge side face is not crucial, only the truncated wedge base sizes are essential. The solution is true for very weak indentation forces only and, therefore, for shallow penetration depths ($h \rightarrow 0$), when the plastic zone and contact on the side wedge faces may be neglected. When solution (7) was derived, it was assumed that contact pressure was evenly distributed, there was no friction and h was assumed as the average displacement value under the punch. Such conditions are not crucial as the difference from the solution for the rigid punch (constant displacements and variable contact pressures) is about 8% [20].

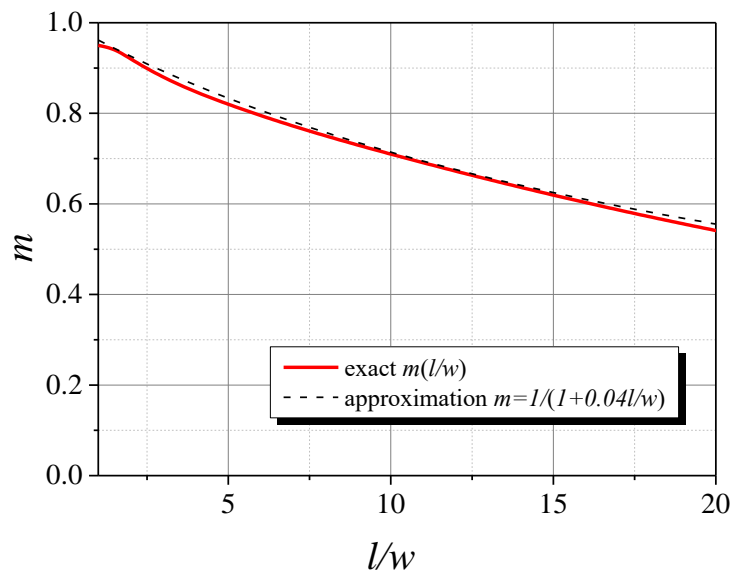


Figure 10. Parameter m in Eq. (7) vs. base side ratio l/w . The simplest approximation of this dependence within the range up to $l/w < 20$ is $m = 1/(1 + 0.04l/w)$

Comparison of Eqs. (7) and (3), get an estimate of the initial indentation curve section slope:

$$k_e = \frac{E}{1-\nu^2} \frac{\sqrt{wl}}{m} \approx \frac{E}{1-\nu^2} \sqrt{wl} \left(1 + \frac{l}{25w} \right). \quad (8)$$

For the considered case with $E = 210$ GPa, $\nu = 0.3$, $w = 381$ μm , $l = 4826$ μm , $m = 0.67$:

$$k_e = 467 \text{ N}/\mu\text{m}. \quad (9)$$

At the stage of *deep* ($h \rightarrow \infty$) indentation of an ideal wedge punch, the solution of the *rigid ideally plastic problem* can be used accounting for geometric similarity of transient plastic flow at plane strain. For the indentation case without friction in [12], the following equation is proposed for the resulting vertical load on the wedge during indentation:

$$F = \frac{4\sigma_Y}{\sqrt{3}} l \frac{(1+\theta)\sin\gamma}{\cos\gamma - \sin(\gamma-\theta)} h. \quad (10)$$

where σ_Y is the yield stress, γ is the wedge half-angle, θ is the angle implicitly defined by the equality $\cos\theta = [\cos\gamma - \sin(\gamma-\theta)][\cos(\gamma-\theta) + \sin\gamma]$ (Fig. 11).

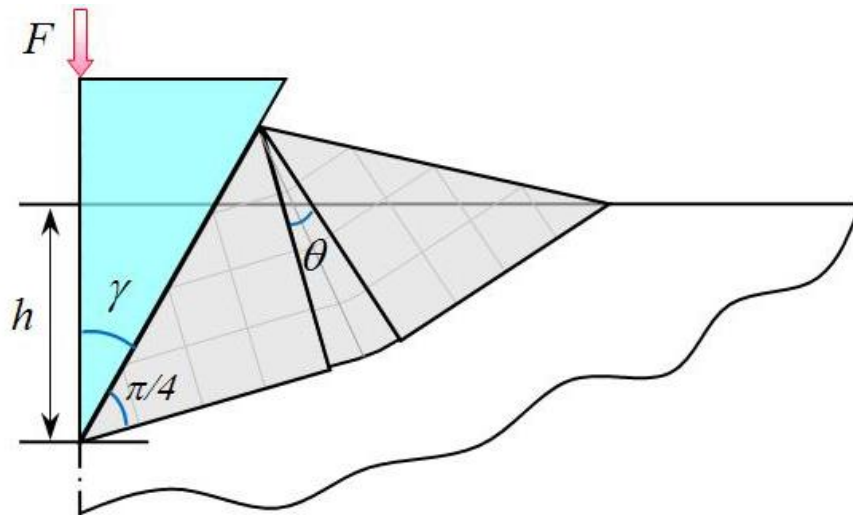


Figure 11. Rigid wedge indentation in half plane. The plastic zone is highlighted in grey

Correlation of Eq. (10) with (6) results in the equation for the final penetration curve section slope:

$$k_p = \frac{4\sigma_Y}{\sqrt{3}} l \frac{(1 + \theta) \sin \gamma}{\cos \gamma - \sin(\gamma - \theta)}. \quad (11)$$

The equation for an ideal wedge with $\sigma_Y = 660 \text{ MPa}$, $l = 4826 \text{ }\mu\text{m}$, $\gamma = 30^\circ$:

$$k_p = 7.41 \text{ N}/\mu\text{m}. \quad (12)$$

Analytic solutions similar to (10) can be derived for the case of wedge indentation with taking into consideration the friction [13, 14, 10]. Curves corresponding to elastic solution (7) and a series of rigid ideal plastic solutions for various friction coefficients μ are shown in Figure 12.

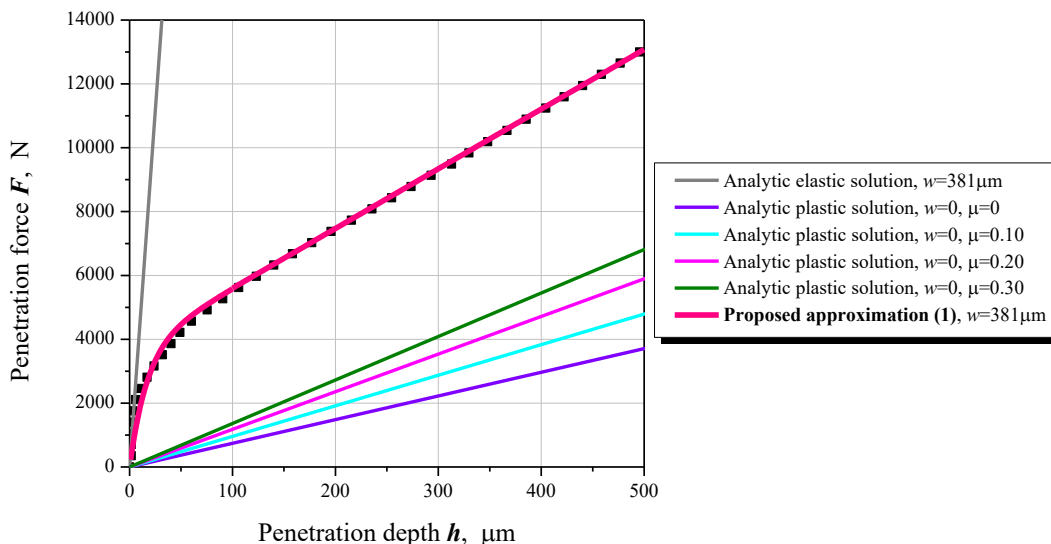


Figure 12. Linear approximations of indentation curve based on analytic elastic and plastic solutions with various values of friction coefficient μ

There are two causes of mismatch of curves plotted based on the ideal plastic solution with the experimental curve shown in Figure 8. First, different geometry: truncated wedge in the experimental studies and ideal (untruncated) wedge in the analytic solution. Truncation additionally contributes to the resulting pressure force acting on the wedge base area, which raises the indentation curve. This is proved by experimental results [22] and FE computations (Fig. 13). The quoted results require

consideration of $F_0(w)$ in model (1). Second, real material hardening that is not considered in the analytic solution obtained based on the ideal plastic model. Comparison of analytic indentation curves for an ideally plastic material with FE solutions (Fig. 14) that consider hardening shows slope increase by 20-30 % due to hardening.

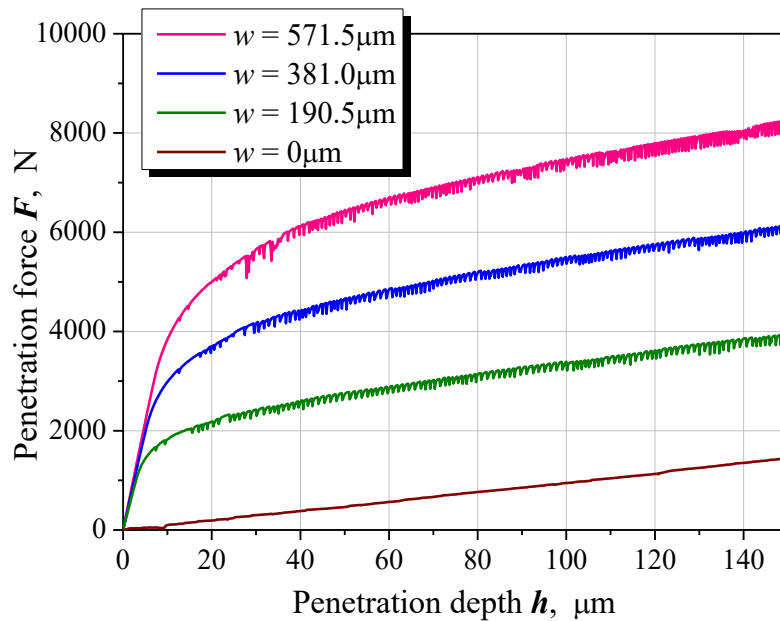


Figure 13. Indentation curves of truncated wedge punches with various base dimensions w plotted based on FE computations ($\mu = 0$)

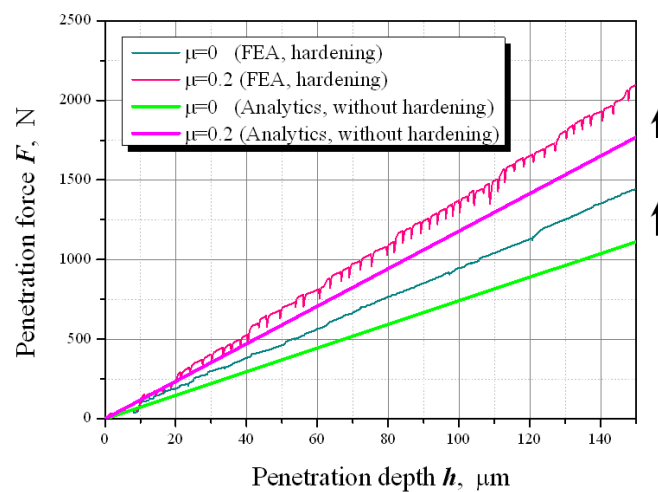


Figure 14. Effect of hardening on the slope of wedge punch indentation curves ($w = 0$)

The analytic solutions of simplified elastic and plastic indentation problems provided above enable to determine the linear character of indentation force dependence on its depth for the studied idealized loading cases and wedge geometry and get explicit dependences of respective slopes of indentation curves on such parameters as E , ν , σ_Y , μ , l , etc. In the general case of truncated wedges and hardening of the indented material, FE computations are required to identify the parameters k_p, F_0 of model (1) that characterize the process of indentation at various developed plastic strains. The parameter k_e that characterizes the initial stage of indentation can be completely determined by Eq. (8).

Identification of k_p and F_0 for a truncated wedge

Assume that the parameters k_p, F_0 depend on the truncated wedge base width w and friction coefficient μ . To identify the specified dependences, multiple computational experiments were performed for four values of $w = 0 \mu\text{m}; 190.5 \mu\text{m}$ (50 % of the standard value); $381 \mu\text{m}$ (100%); $571.5 \mu\text{m}$ (200%) and three values of $\mu = 0; 0.2; 0.4$. The results of computations are shown in Figure 15.

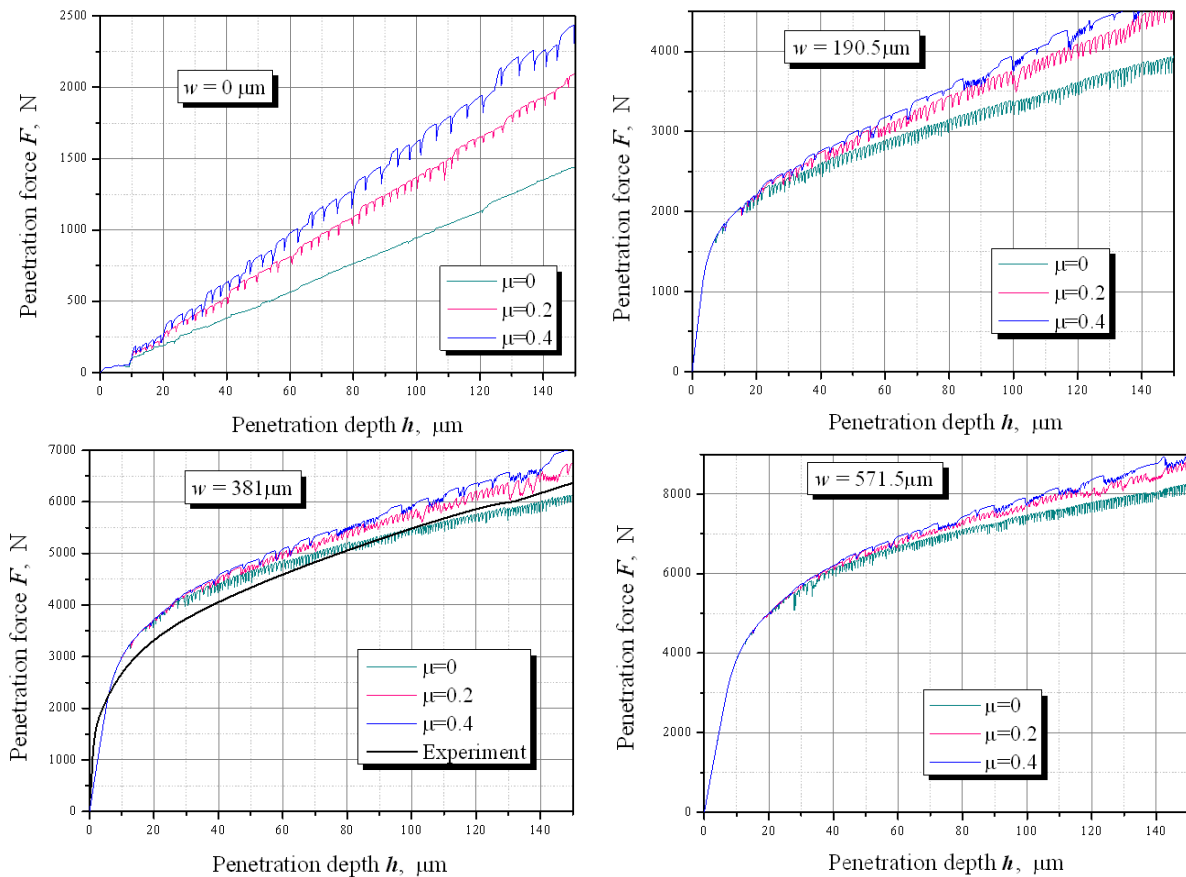


Figure 15. Indentation curves of a wedge punch with various base dimensions w and values of friction coefficient μ plotted based on FE computation results

The model of an elastic-plastic body with nonlinear hardening (see for details [15-17, 23, 24]) was used for FE computations. The experimental stress-strain curve is shown in Figure 16. It is plain that its ideally plastic approximation is crude enough. Computations were made by multiplicative decomposition of the strain gradient into elastic and plastic parts. Dissipation along the contact line due to the Coulomb friction was considered along with volume plastic dissipation.

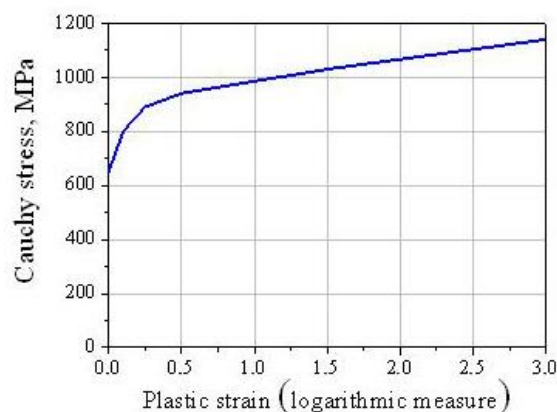


Figure 16. Stress-strain curve used in FE computations

An indentation in computational experiments was modelled by rigid indenters with various wedge base width values. Computations were made under assumption of the plane strain conditions. The results of computations are provided in Figure 17.

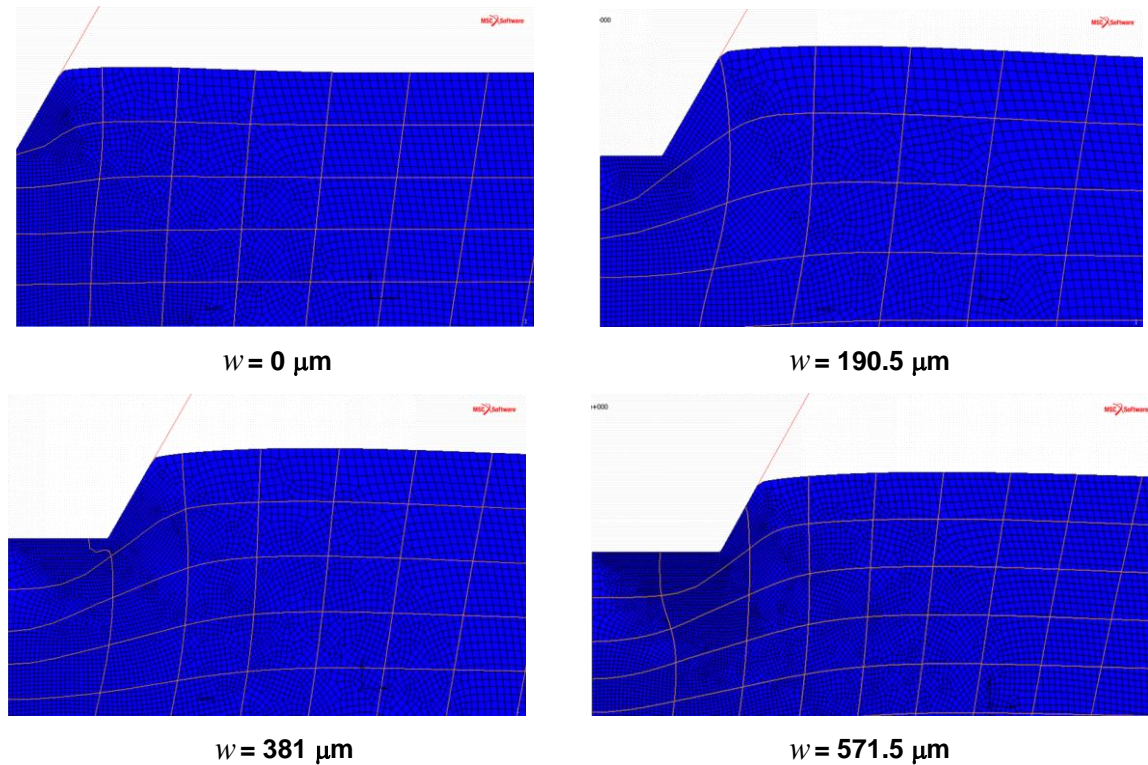


Figure 17. Deformed states after indentation of wedge punches with various base dimensions w

The slopes of asymptote k_p and the heights of asymptote intersection with Y-axis determined based on the calculated indentation curves presented in Fig. 9 are provided in Tables 1 and 2.

Table 1. Slopes of asymptote k_p [N/μm] vs. wedge base width w and friction coefficient μ

	$\mu = 0$	$\mu = 0.2$	$\mu = 0.4$
$w = 0 \mu\text{m}$	9.66	13.9	16.4
$w = 190.5 \mu\text{m}$	12.3	16.7	18.7
$w = 381.0 \mu\text{m}$	15.6	19.3	21.4
$w = 571.5 \mu\text{m}$	18.1	21.8	23.5

Table 2. Heights of asymptote intersection with Y-axis F_0 [N] vs. wedge base width w and friction coefficient

	$\mu = 0$	$\mu = 0.2$	$\mu = 0.4$
$w = 0 \mu\text{m}$	0	0	0
$w = 190.5 \mu\text{m}$	2095	2029	2013
$w = 381.0 \mu\text{m}$	3835	3787	3748
$w = 571.5 \mu\text{m}$	5548	5481	5469

The graphic presentation of the parameters k_p and F_0 is shown in Figure 18.

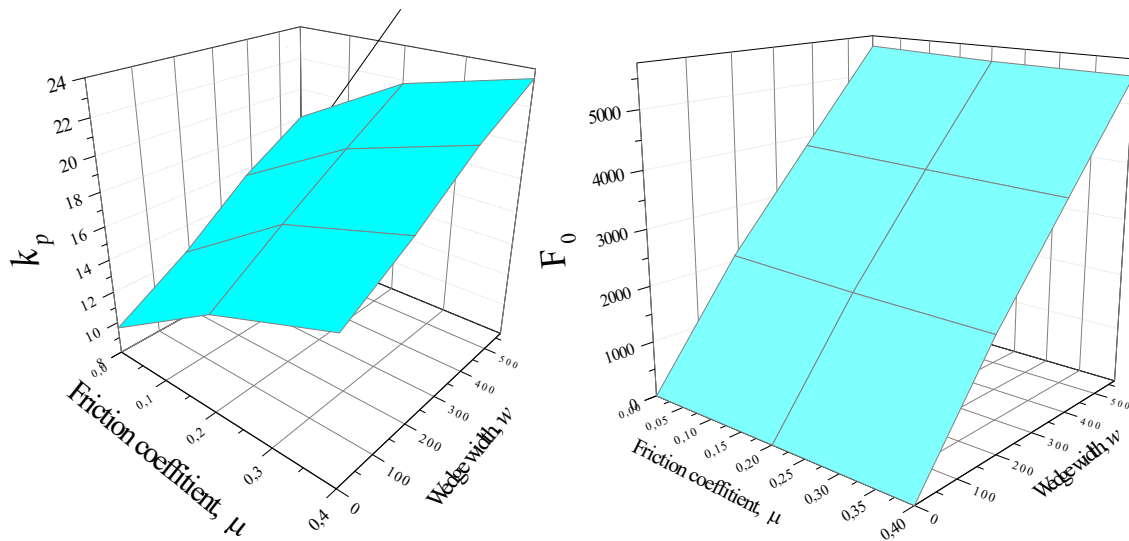


Figure 18. Dependences of $k_p(w, \mu)$ and $F_0(w, \mu)$

Constants of bilinear, biquadratic and mixed approximation of $k_p(w, \mu)$ and $F_0(w, \mu)$ were determined using the least square method.

For *bilinear* approximation

$$k_p = A + Bw + C\mu \quad (13)$$

the constants take the following values

$$\begin{aligned} A &= 10.2915 \text{ N}/\mu\text{m} \\ B &= 0.01381 \text{ N}/\mu\text{m}^2 \\ C &= 15.2125 \text{ N}/\mu\text{m} \end{aligned} \quad (14)$$

The root mean square (RMS) error in this case is $\chi=0.358$.

For *biquadratic* approximation

$$k_p = A + Bw + C\mu + Dw^2 + Q\mu^2 + Pw\mu \quad (15)$$

the constants take the following values

$$\begin{aligned} A &= 9.56917 \text{ N}/\mu\text{m} \\ B &= 0.01586 \text{ N}/\mu\text{m}^2 \\ C &= 26.62 \text{ N}/\mu\text{m} \\ D &= -1.4696 \cdot 10^{-6} \text{ N}/\mu\text{m}^3 \\ Q &= -24.1875 \text{ N}/\mu\text{m} \\ P &= -0.00606 \text{ N}/\mu\text{m}^2 \end{aligned} \quad (16)$$

The RMS error in this case is $\chi=0.0267$.

For *mixed* approximation

$$k_p = A + Bw + C\mu + D\mu^2 \quad (17)$$

the constants take the following values

$$\begin{aligned}
 A &= 9.969 \quad \text{N}/\mu\text{m} \\
 B &= 0.01381 \quad \text{N}/\mu\text{m}^2 \\
 C &= 24.89 \quad \text{N}/\mu\text{m} \\
 D &= -24.19 \quad \text{N}/\mu\text{m}
 \end{aligned}
 \tag{18}$$

The RMS error in this case is $\chi=0.0810$.

The dependence $F_0(w, \mu)$ (Fig. 12) demonstrates almost total absence of μ effect on F_0 , and the dependence $F_0(w)$ is close to linear, therefore, assume that

$$F_0 = G + Hw, \tag{19}$$

where the best values of constants are as follows

$$\begin{aligned}
 G &= 95 \quad \text{N} \\
 H &= 9.6 \quad \text{N}/\mu\text{m}
 \end{aligned}
 \tag{20}$$

It should be noted that constant G is small as compared to the observed levels of F (thousands and tens of thousands Newton) and it may be neglected.

The constants from (14), (16), (18), (20) fit the case of $l = 4826 \mu\text{m}$ and should be changed proportionally to the changes in the wedge base length l .

Visual analysis of functions $k_p(w, \mu)$ (Fig. 12) demonstrates that dependence $k_p(w)$ is very close to linear, while $k_p(\mu)$ is nonlinear. Therefore mixed approximation (17) will be further considered as the principal one. Usage of approximations (17) and (19) is equivalent to development of an indentation model based on two hypotheses:

Linear dependence of slope k_p and shear in Y direction F_0 on the base width w ;

Quadratic dependence of slope k_p and independence of F_0 from the friction coefficient μ .

Thus, based on (17) and (19), approximation (1) can be presented as

$$F(h; w, \mu) = \left[(A + Bw + C\mu + D\mu^2)h + G + Hw \right] \left(1 - e^{-\frac{k_e}{G+Hw}h} \right). \tag{21}$$

Comparison of approximation (21) with results of FE computations demonstrated (Fig. 19) good accuracy in a wide range of the parameters w and μ .

Dependences $F(h, \mu)$ at four different values of w and $F(h, w)$ and three values of μ demonstrate (Fig. 20) that w has a dominant impact on the indentation force of the two considered parameters w and μ . If the friction coefficient μ has a fixed value, approximation (21) will be simplified:

$$F(h; w) = \left[(A + Bw)h + G + Hw \right] \left(1 - e^{-\frac{k_e}{G+Hw}h} \right). \tag{22}$$

If the base width value w is fixed, approximation (21) takes the following form:

$$F(h; \mu) = \left[(A + C\mu + D\mu^2)h + G \right] \left(1 - e^{-Qh} \right). \tag{23}$$

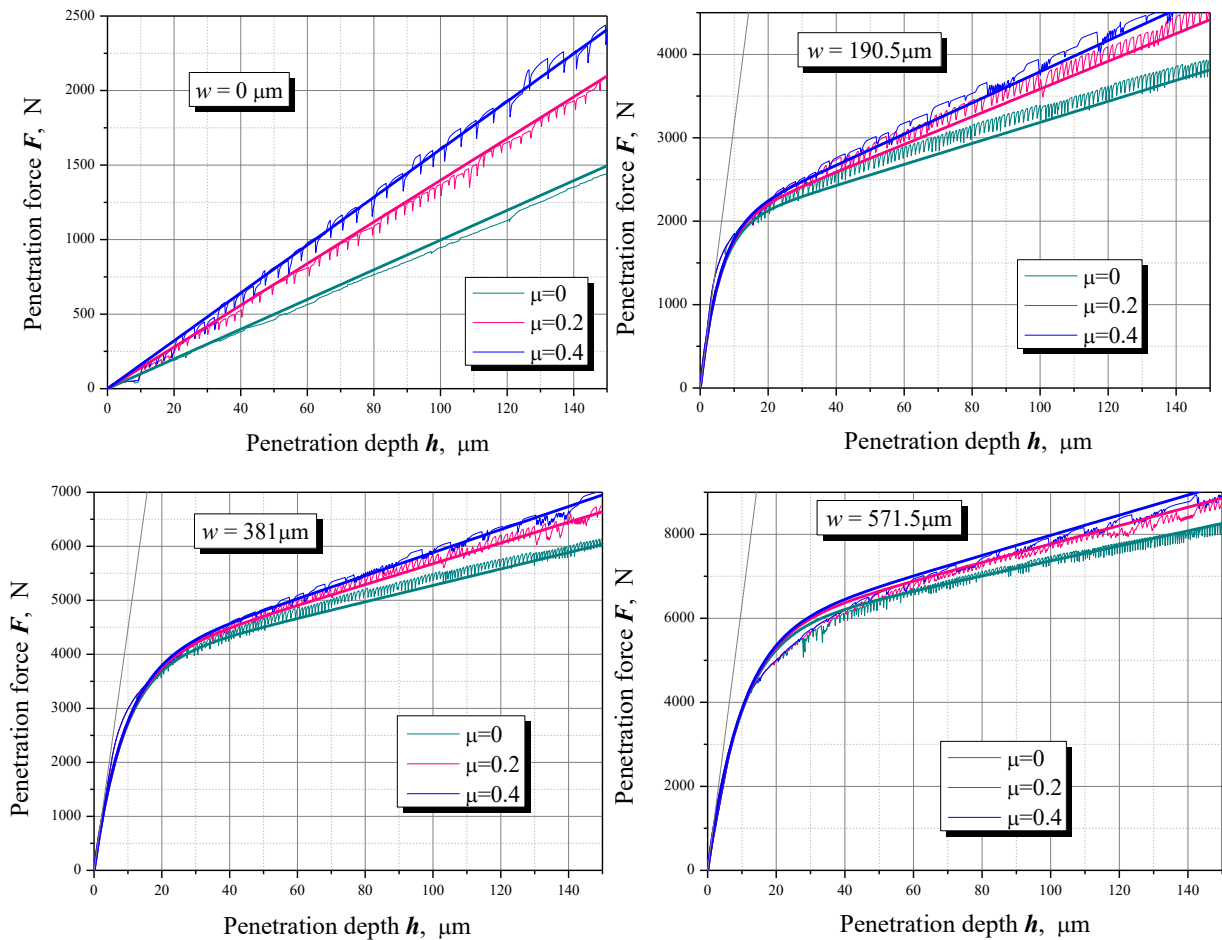


Figure 19. Comparison of calculated wedge punch indentation curves with approximation (21) (thick lines) at various base dimensions w and friction coefficients

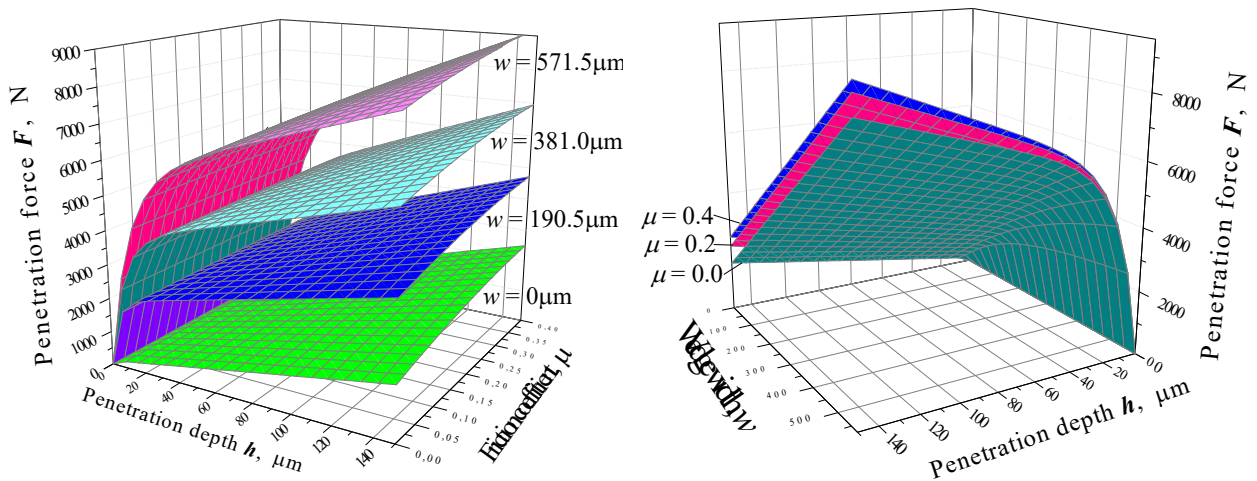


Figure 20. Parametric analysis of approximation (21)

The size of the area of the nonlinear (transition) indentation curve section at the deviation from the linear approximation of $\delta = 1\%$, neglecting G and assuming that k_e is constant, can be roughly estimated based on the relationship

$$h_{\delta=1\%} \approx -\frac{H \ln 0.01}{k_e} w \approx w/10. \quad (24)$$

If the deviation from the linear approximation $\delta=0.1\%$:

$$h_{\delta=0.1\%} \approx -\frac{H \ln 0.001}{k_e} w \approx w/7. \quad (25)$$

For a more accurate estimate, the following equation should be used

$$h_{\delta} = -\frac{1-\nu^2}{E} m \frac{(Hw + G) \ln \delta}{\sqrt{wl}}. \quad (26)$$

For the set of parameters $E = 210 \text{ GPa}$, $\nu = 0.3$, $w = 381 \text{ }\mu\text{m}$, $l = 4826 \text{ }\mu\text{m}$, $m = 0.67$, obtain $h_{\delta=1\%} = 37 \text{ }\mu\text{m}$ and $h_{\delta=0.1\%} = 55 \text{ }\mu\text{m}$.

To determine the coefficients of Eq. (21), both experimental and FE results can be used.

Subject to the plane strain state condition ($w \ll l$), it is possible to consider the dependence on l explicitly and use the following approximation instead of (17) to calculate k_p

$$k_p = (\bar{A} + \bar{B}w + \bar{C}\mu + \bar{D}\mu^2)l, \quad (27)$$

where the constants are obtained by dividing the values of constants from (18) by $l = 4826 \text{ }\mu\text{m}$:

$$\begin{aligned} \bar{A} &= 0.207 & \text{N}/\mu\text{m}^2 \\ \bar{B} &= 0.00000286 & \text{N}/\mu\text{m}^3 \\ \bar{C} &= 0.00516 & \text{N}/\mu\text{m}^2 \\ \bar{D} &= -0.00501 & \text{N}/\mu\text{m}^2 \end{aligned} \quad (28)$$

Eq. (19) can be modified for F_0 in a similar way

$$F_0 = (\bar{G} + \bar{H}w)l, \quad (29)$$

where the constants take the following values

$$\begin{aligned} \bar{G} &= 0.0197 & \text{N}/\mu\text{m} \\ \bar{H} &= 0.00199 & \text{N}/\mu\text{m}^2 \end{aligned} \quad (30)$$

Based on the obtained results (27) and (29) and the explicit equation of k_e in terms of w and l (8), if $1/20 < w/l \ll 1$, the following formula should be used instead of (21):

$$F(h; w, l, \mu) = \left[(\bar{A} + \bar{B}w + \bar{C}\mu + \bar{D}\mu^2)h + \bar{G} + \bar{H}w \right] l \left(1 - e^{-\frac{E}{1-\nu^2} \sqrt{wl} \left(1 + \frac{l}{25w} \right) \frac{h}{\bar{G} + \bar{H}w}} \right). \quad (31)$$

Identification of parameter k_p for untruncated (ideal) wedges

Symmetric untruncated wedges (Fig. 21a) can be considered as a special case of symmetric truncated wedges at $w=0$ (see Fig. 2). Unsymmetric untruncated wedges (Fig. 21b) should be considered separately. However, based on the experimental and FE computations data, both cases allow for linear approximation (6)

$$F = k_p h. \quad (6)$$

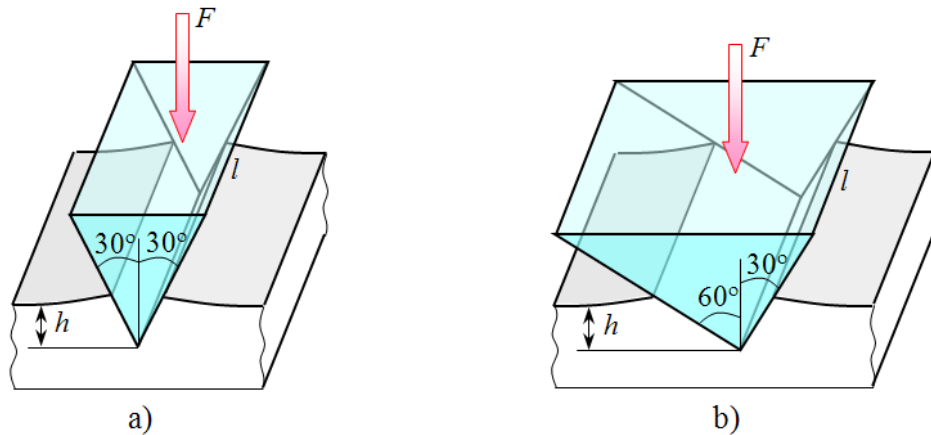


Figure 21. Symmetric (a) and unsymmetric (b) untruncated (ideal) wedges

It is assumed that the parameter k_p depends on the friction coefficient μ . Computational experiments were performed to identify the above dependence for three values of $\mu = 0; 0.2; 0.4$. The results of FE computations are provided in Figure 22.

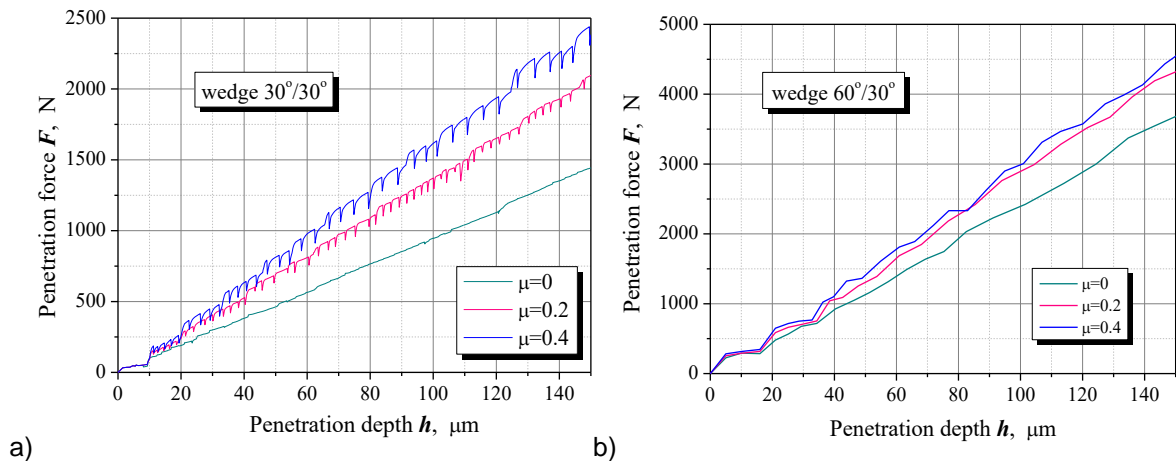


Figure 22. Indentation curves of symmetric (a) and unsymmetric (b) untruncated wedge punches at various friction coefficients μ , obtained using FE method

The model of an elastic-plastic body with nonlinear hardening was used for the indented material in FE computations. The strain diagram obtained from experiments and used for computations is shown in Fig. 16. A rigid indenter was used for indentation. Computations were based on the plane strain state hypothesis. Computation results are shown in Figure 23.

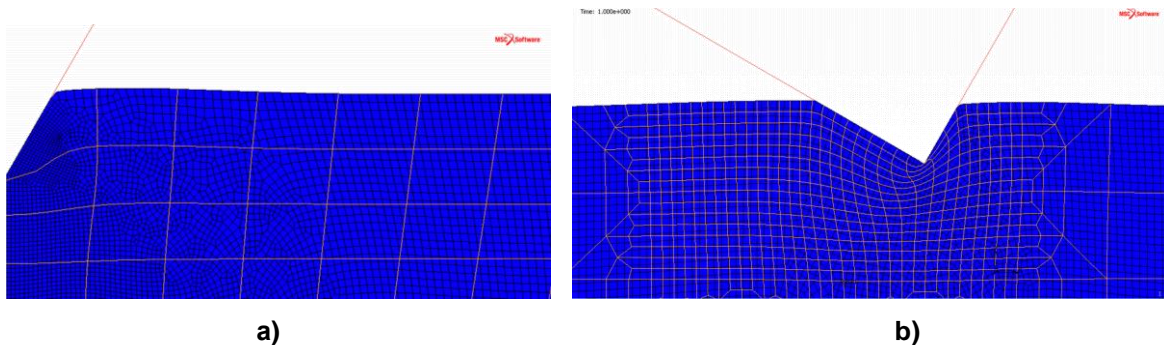


Figure 23. Strain state during indentation of a symmetric (a) and unsymmetric (b) untruncated wedge punches

The asymptote k_p slope values determined by the predicted indentation curves shown in Figure 22 are provided in Table 3.

Table 3. Asymptote k_p [N/ μ m] slope values vs. friction coefficient μ .

	$\mu = 0$	$\mu = 0.2$	$\mu = 0.4$
Symmetric wedge 30°/30°	9.55	13.7	16.1
Unsymmetric wedge 60°/30°	24.2	28.6	29.9

The graphic representation of the parameter k_p vs. μ is shown in Fig. 24. Dependences for symmetric and unsymmetric wedges are practically similar. The only significant difference is the height of the intersection point with Y-axis.

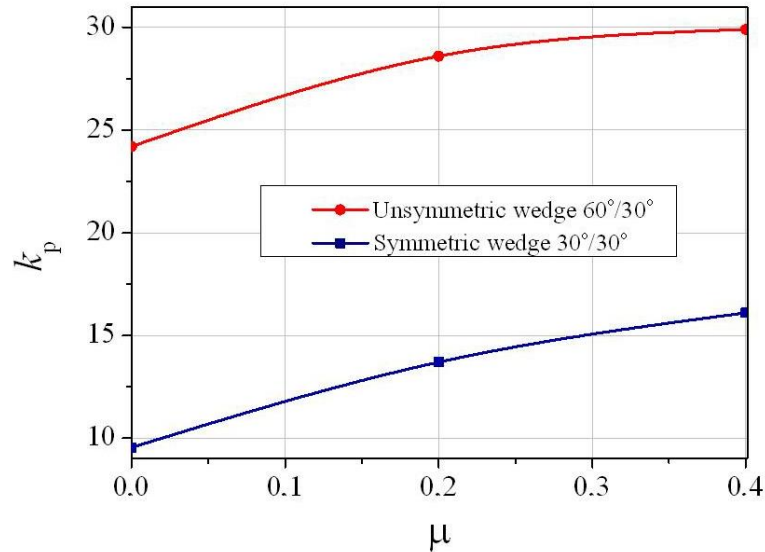


Figure 24. Dependence $k_p(\mu)$

The quadratic approximation constants $k_p(\mu)$ were determined using the least square method:

$$k_p = A + C\mu + D\mu^2 \tag{32}$$

the constant values for a symmetric wedge are:

$$\begin{aligned} A_{30/30} &= 9.55 && \text{N}/\mu\text{m} \\ C_{30/30} &= 25.13 && \text{N}/\mu\text{m} \\ D_{30/30} &= -21.88 && \text{N}/\mu\text{m} \end{aligned} \tag{33}$$

the constant values for an unsymmetric wedge are:

$$\begin{aligned} A_{60/30} &= 24.20 && \text{N}/\mu\text{m} \\ C_{60/30} &= 29.75 && \text{N}/\mu\text{m} \\ D_{60/30} &= -38.75 && \text{N}/\mu\text{m} \end{aligned} \tag{34}$$

The above constants are valid for $l = 4826 \mu\text{m}$ and should be changed proportionately to the changes in the wedge base length l .

Some difference of the constant values (33) as compared to (18) (also describing the untruncated wedge behavior at $w=0$) is due to the fact that the constants (18) were obtained from a wider calculations database that accounts for w variations and therefore provides a less correct prediction for the case under consideration.

Semenov A.S., Semenov S.S., Melnikov B.E, Tikhonov V.S. Modeling of indentation and slip of wedge punch. *Magazine of Civil Engineering*. 2017. No. 6. Pp. 78–101. doi: 10.18720/MCE.74.8

Based on (32), approximation (6) can be rewritten as

$$F(h; \mu) = (A + C\mu + D\mu^2)h \quad (35)$$

It is obvious that Eq. (35) can be considered as a special case of function (21).

Comparison of approximation (35) with FE computation data showed (Fig. 25) good accuracy in a wide range of parameter μ variation.

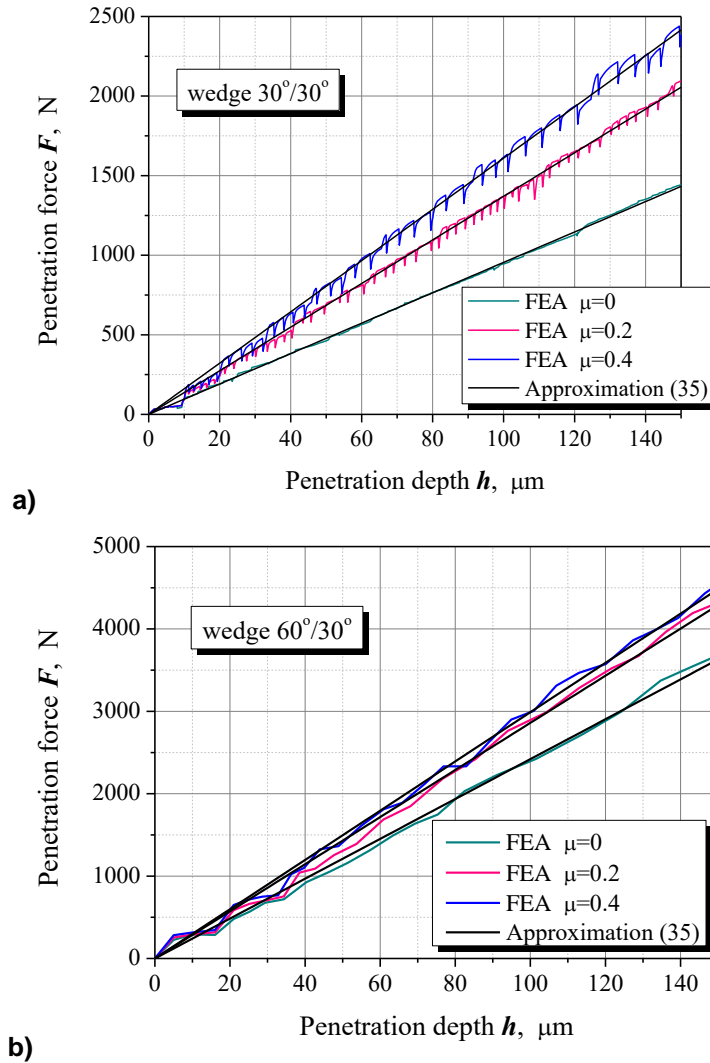


Figure 25. Comparison of predicted indentation curves of symmetric (a) and unsymmetric (b) untruncated wedge punches with approximation (35) at various friction coefficients μ .

Subject to the plane strain state condition ($w \ll l$), it is possible to consider the dependence on the wedge length l explicitly and use the following approximation instead of (23) to calculate k_p

$$k_p = (\bar{A} + \bar{C}\mu + \bar{D}\mu^2)l, \quad (36)$$

where the constants are obtained by dividing the values of constants from (33) and (34) by $l = 4826 \mu\text{m}$. For a symmetric wedge, such constants are as follows:

$$\begin{aligned} \bar{A}_{30/30} &= 0.00198 & \text{N}/\mu\text{m}^2 \\ \bar{C}_{30/30} &= 0.00521 & \text{N}/\mu\text{m}^2 \\ \bar{D}_{30/30} &= -0.00453 & \text{N}/\mu\text{m}^2 \end{aligned} \quad (37)$$

and for an unsymmetric wedge, such constants are as follows:

$$\begin{aligned}\bar{A}_{60/30} &= 0.00501 & \text{N}/\mu\text{m}^2 \\ \bar{C}_{60/30} &= 0.00616 & \text{N}/\mu\text{m}^2 \\ \bar{D}_{60/30} &= -0.00803 & \text{N}/\mu\text{m}^2\end{aligned}\quad (38)$$

If approximation (32) is substituted by (36), the following equation that comprises explicit dependence on the wedge length l can be considered instead of (35):

$$F(h; l, \mu) = (\bar{A} + \bar{C}\mu + \bar{D}\mu^2)hl. \quad (39)$$

It should be noted that both experimental and FE computation data can be used to determine constants of Eqs. (35) and (39). Approximation (39) is valid only if $w \ll l$ and its factors can be obtained using 2D FE analysis.

Results of FE modeling of slip of indented tooth

Obtaining of universal analytical estimations to describe the transient indented tooth slip process is an independent and quite difficult problem. Such problem is confined below to consideration of 3D FE modeling of the single tooth slip and experimental data. In future they can be useful for development of an analytical tooth breakaway force model.

Figures 26 and 27 show the results of FE computations of single tooth indentation to a depth of $150 \mu\text{m}$ with its further slip. The problem was solved for the symmetric case.

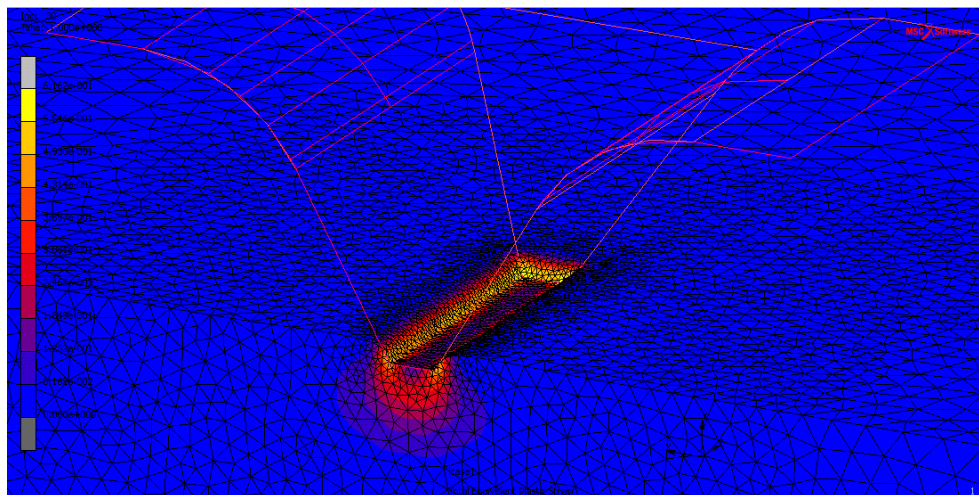


Figure 26. Plastic strain intensity field distribution during tooth indentation

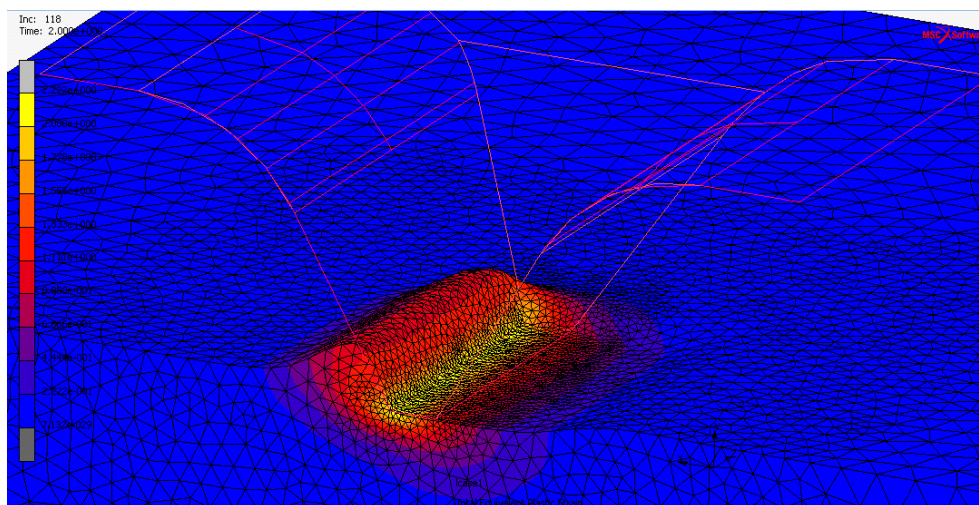


Figure 27. Plastic strain intensity field distribution during indented tooth slip

According to the figures, the material is subjected to a considerable plastic strain when a bed is formed in front of the slipping wedge even at shallow indentation depths. The effect of the side edge and 3D strain is shown in Figure 27. It results in a smaller bed formed in front of the tooth near the side edge, besides an additional lateral face is formed where tribological phenomena are also taking place.

Figure 28 shows tooth slip diagrams drawn based on 2D and 3D FE solutions. The tooth was assumed to be a rigid body. Oscillations on the assumption slip diagrams are attributable to inhomogeneity of the dynamic process of slipping during shear. It should be noted that similar oscillations are also present on the experimental diagrams (see Fig. 4). Figure 28 shows a smooth monotone approximation derived by averaging of several tests results. The comparison of the solutions in 2D and 3D statements enables to assess the effect of side edges and 3D strain state close to such edges. Such effect does not exceed 10 %.

The solution of this boundary value problem accounting for the nonlinearities of three types (plasticity, finite strains, and contact with friction) requires effective computation methods [24], detailed spatial discretization and a considerable amount of time increments for convergence of iterative procedures. The geometrically nonlinear problems were solved using FE software MSC.Marc [25]. The Lagrange updated formulation was used. The model of elastic-plastic body with nonlinear hardening was used for the indented material in FE computations (Fig. 16). Computations included multiplicative decomposition of the strain gradient into the elastic and plastic parts.

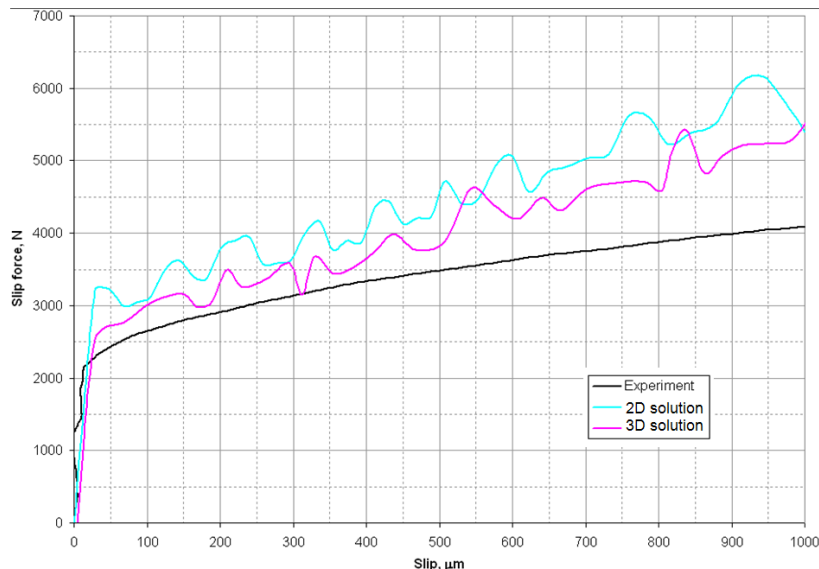


Figure 28. Single tooth shear diagrams

The comparison of the computational and experimental shear diagrams demonstrated satisfactory accuracy (less than 15 % for the shear of up to 500 μm), therefore the computational diagrams may be used as the basis for assessment of the punch indentation force and punch breakaway drag force during its shearing as a function of indentation depth. A limitation of such approach is the need to perform new FE computations for each new punch size, configuration and each material grade. This requires development of universal analytical models to describe the slip process similar to those proposed above (see e.g. (35), (40), (41)) to describe the indentation process.

Discussion

The results of analytical [12-14, 20, 21, etc.] and experimental [9-11, 6, 5, etc.] studies of the processes of teeth indentation in to the elastic [20, 21, etc.] and plastic [12-14, etc.] continuum are widely presented in the literature. However, there is no unified model of deep and shallow indentation processes of an ideal and non-ideal wedge-shaped punch, taking into account the dependence of force on the depth of the indented die, its geometry, plastic hardening of material and lateral friction, which is oriented to the determining the load bearing capacity of gripping devices for drillpipes. In this paper, an attempt is made to construct a similar unified model based on the unification and generalization of known analytical solutions, as well as identification of model parameters based on multivariant finite element computations and its experimental verification.

The proposed analytic dependence of the indentation force of an ideal and non-ideal wedge-shaped tooth with symmetrically sloped sides (30°) and unsymmetrically sloped sides (30°/60°) modeling

tooth operation as a function of indentation depth and friction coefficient on the punch lateral face both for shallow and deep indentation is determined *in general case* by the expression:

$$F(h; w, \mu) = \left[(A + Bw + C\mu + D\mu^2)h + G + Hw \right] \left(1 - e^{-\frac{k_e}{G+Hw}h} \right). \quad (21)$$

Simplified version of (21) in the form of the linear approximation (6) can be used to analyze the process of indentation of *ideal (untruncated)* symmetric and unsymmetric wedges, which in expanded form (35) allows for the following representation:

$$F(h; \mu) = (A + C\mu + D\mu^2)h, \quad (35)$$

which constants are determined according to (33) for a symmetric wedge and according to (34) for an unsymmetric wedge. An analogous (linear in respect to h) dependence is considered in [13].

Linear approximation (2) can be used to describe the process of *non-ideal (truncated)* wedge indentation to *considerable depths* ($h > w/7$, where h is the indentation depth, w is the truncated wedge base width), which in expanded form (obtained for special case (21) at high h/w values) can be rewritten as:

$$F(h; w, \mu) = (A + Bw + C\mu + D\mu^2)h + G + Hw, \quad (40)$$

where the constants for a symmetric wedge are determined according to (18)-(20).

Nonlinear approximation (1) should be used to analyze the process of truncated wedge indentation to *shallow depths* ($h < w/7$), which in expanded form (obtained for special case (31) at low h/w) can be rewritten as:

$$F(h; w, \mu) = \left[(A + Bw + C\mu + D\mu^2)h + G + Hw \right] \left(1 - e^{-\frac{Q\sqrt{w}}{G+Hw}h} \right), \quad (41)$$

where $Q = 23.9 \text{ N}/\mu\text{m}^{3/2}$ and the remaining constants A, B, C, D, G, H are the same as the above factors for considerable indentation depths (18)-(20).

The form of introduced approximations is based on the analysis of experimental indentation curves and analytic solutions of the boundary value elasticity and plasticity problems. The constants of the introduced approximations were obtained by the least square method based on the results of multiple FE computations and agree with the available experimental data. The ranges of the valid argument variations, for which the approximation is kept interpolational are:

$$\begin{aligned} 0 \mu\text{m} &\leq h \leq 150 \mu\text{m}, \\ 0 \mu\text{m} &\leq w \leq 571.5 \mu\text{m}, \\ 0 &\leq \mu \leq 0.4. \end{aligned}$$

The wedge base length l and the wedge half-angle γ were assumed fixed $l = 4826 \mu\text{m}$, $\gamma = 30^\circ$ to determine the approximation factors. Subject to the condition $w \ll l$, it is possible to use the approximation that explicitly provides for the dependence on l , as (39) for untruncated and (31) for truncated wedges. Cases with $\gamma \neq 30^\circ$ require further study, which can be performed in a similar way, if necessary, based on multiple computational experiments.

Conclusion

A simplified analytical model was proposed to determine the indentation force of an ideal (untruncated) and non-ideal (truncated) wedge punch with symmetrically sloped sides (30°) and unsymmetrically sloped sides ($30^\circ/60^\circ$) modeling tooth operation as a function of indentation depth and friction coefficient on the punch lateral face both for shallow (mostly typical of elastic strain) and deep (mostly typical of plastic strain) indentation. The developed models closely agree with the FE analysis and experimental data.

The FE modeling of single tooth indentation and slip was performed with using 2D and 3D models. The comparison of the computational slip diagrams with the experimental data demonstrated satisfactory accuracy, therefore such computational diagrams may be used as a basis for assessment of punch indentation, breakaway and drag forces during its shearing as a function of the indentation depth.

The obtained results can be used to develop a holding force model for a multi-tooth slip.

Acknowledgement

The research was carried out on the contract of Weatherford and supported also by the Russian Foundation for Basic Research (grant no. 16-08-00845).

References

1. Saroian A.E. *Teoriia i praktika raboty buril'noi kolonny*. [Theory and practice of drill string operation] M.: Nedra, 1990. 263 p. (rus)
2. Spiri W.H., Reinhold W.B. Why does drill pipe fail in the slip area? *World Oil*. 1959. October. Pp. 100-115.
3. Paslay P., Pattillo P.D., Pattillo D. II, Sathuvalli U.B.R., Payne M.L. A re-examination of Drillpipe/Slip Mechanics. *Proceedings of the IADC/SPE Drilling Conference, Miami, Florida*. 2006. Paper IADC/SPE 99074. Pp. 1-8.
4. Jayadevan K.R., Narasimhan R. Finite element simulation of wedge indentation. *Computers & Structures*. 1995. No. 5(57). Pp. 915-927.
5. Mitsomwang P., Natpukkana P., Borrisutthekul R., Nagasawa S. Effects of blade tip geometry on cutting characteristics of lead alloy sheet subjected to wedge indentation. *Key Engineering Materials*. 2017. Vol. 719. Pp. 137-141.
6. Kim W., Kawai K., Koyama H. Metal flow in wedge indentation of V- and W-shaped tools. *Journal of Materials Processing Technology*. 2007. No. 1(189). Pp. 392-400.
7. Voyiadjis G.Z., Buckner N.E. Indentation of a half-space with a rigid indenter. *Int. J. Numer. Methods Engrg*. 1983. No. 10(19). Pp. 1555-1578.
8. Bucaille J.L., Felder E., Hochstetter G. Mechanical analysis of the scratch test on elastic and perfectly plastic materials with the three-dimensional finite element modeling. *Wear*. 2001. No. 5(249). Pp. 422-432.
9. Dugdale D.S. Wedge indentation experiments with cold-worked metals. *Journal of the Mechanics and Physics of Solids*. 1953. No. 1(2). Pp. 14-26.
10. Grunzweig J., Longman I.M., Petch N.J. Calculations and measurements on wedge-indentation. *J. Mechanics and Physics of Solids*. 1954. No. 2(2). Pp. 81-86.
11. Kailas S.V., Biswas S.K. Material response to two-dimensional scratching by wedges. *Wear*. 1993. Vol. 162. Pp. 110-118.
12. Hill R., Lee E.H., Tupper S.J. The theory of wedge indentation of ductile materials. *Proc. of the Royal Society of London. Series A, Mathematical and Physical Sciences*. 1947. No. 1013(188). Pp. 273-289.
13. Sokolovskii V.V. *Teoriia plastichnosti* [Theory of plasticity]. 1969. Moscow: «Vysshaya shkola». 608 p. (rus)
14. Nepershin R.I. Vnedrenie konechnogo klina v ideal'noplasticheskoe poluprostranstvo [Indentation of a finite wedge into an ideally plastic half-space]. *Izvestiia Rossiiskoi Akademii Nauk. Mekhanika tverdogo tela*. 2003. No. 4. Pp. 176-183. (rus)
15. Melnikov B.E., Semenov A.S. Creation and application of hierarchical sequence of material models for numerical analysis of elasto-plastic structures. *Zeitschrift für Angewandte Mathematik und Mechanik*. 1996. No. S2(76). Pp. 615-616.
16. Semenov A., Melnikov B. Interactive rheological modeling in elasto-visco-plastic finite element analysis. *Procedia*

Литература

1. Сароян А.Е. Теория и практика работы бурильной колонны. М.: Недра, 1990. 263 с.
2. Spiri W.H., Reinhold W.B. Why does drill pipe fail in the slip area? // *World Oil*. 1959, October. Pp. 100-115.
3. Paslay P., Pattillo P.D., Pattillo D., Sathuvalli U.B.R., Payne M.L. A re-examination of Drillpipe/Slip Mechanics // *Proceedings of the IADC/SPE Drilling Conference, Miami, Florida*. 2006. Paper IADC/SPE 99074. Pp. 1-8.
4. Jayadevan K.R., Narasimhan R. Finite element simulation of wedge indentation // *Computers & Structures*. 1995. № 5(57). Pp. 915-927.
5. Mitsomwang P., Natpukkana P., Borrisutthekul R., Nagasawa S. Effects of blade tip geometry on cutting characteristics of lead alloy sheet subjected to wedge indentation // *Key Engineering Materials*. 2017. Vol. 719. Pp. 137-141.
6. Kim W., Kawai K., Koyama H. Metal flow in wedge indentation of V- and W-shaped tools // *Journal of Materials Processing Technology*. 2007. № 1(189). Pp. 392-400.
7. Voyiadjis G.Z., Buckner N.E. Indentation of a half-space with a rigid indenter // *Internat. J. Numer. Methods Engrg*. 1983. № 10(19). Pp. 1555-1578.
8. Bucaille J.L., Felder E., Hochstetter G. Mechanical analysis of the scratch test on elastic and perfectly plastic materials with the three-dimensional finite element modeling // *Wear*. 2001. № 5(249). Pp. 422-432.
9. Dugdale D.S. Wedge indentation experiments with cold-worked metals // *Journal of the Mechanics and Physics of Solids*. 1953. № 1(2). Pp. 14-26.
10. Grunzweig J., Longman I.M., Petch N.J. Calculations and measurements on wedge-indentation // *J. Mechanics and Physics of Solids*. 1954. № 2(2). Pp. 81-86.
11. Kailas S.V., Biswas S.K. Material response to two-dimensional scratching by wedges // *Wear*. 1993. Vol. 162. Pp. 110-118.
12. Hill R., Lee E.H., Tupper S.J. The theory of wedge indentation of ductile materials // *Proc. of the Royal Society of London. Series A, Mathematical and Physical Sciences*, 1947. № 1013(188). Pp. 273-289.
13. Соколовский В.В. Теория пластичности. М.: «Вышш. школа», 1969. 608 с.
14. Непершин Р.И. Внедрение конечного клина в идеальнопластическое полупространство // *Известия Российской Академии Наук. Механика твердого тела*. 2003. № 4. С. 176-183.
15. Melnikov B.E., Semenov A.S. Creation and application of hierarchical sequence of material models for numerical analysis of elasto-plastic structures // *Zeitschrift für Angewandte Mathematik und Mechanik*. 1996. № S2(76). Pp. 615-616.
16. Semenov A., Melnikov B. Interactive rheological modeling in elasto-visco-plastic finite element analysis // *Procedia Engineering*. 2016. Vol. 165. Pp. 1748-1756.
17. Semenov A.S., Melnikov B.E., Gorokhov M.Y. About the

Семенов А.С., Семенов С.Г., Мельников Б.Е., Тихонов В.С. Моделирование внедрения и сдвига штампа клиновидной формы // *Инженерно-строительный журнал*. 2017. № 6(74). С. 78-101.

- Engineering*. 2016. Vol. 165. Pp. 1748-1756.
17. Semenov A.S., Melnikov B.E., Gorokhov M.Y. About the causes of cyclical instability at computations of large elasto-plastic strains. *Proc. SPIE*. 2005. Vol. 5831. Pp. 167-173.
 18. Pavlov P.A., Ainabekov A.I., Raimberdiev T.P., Mel'nikov B.E. *Dlitel'naia prochnost' staley v usloviakh slozhnogo i termomekhanicheskogo nagruzheniia*. Almaty: Fylym. 1996. 247 p. (rus)
 19. Melnikov B.E., Semenov A.S. Fatigue damage accumulation under the complex varying loading. *Applied Mechanics and Materials*. 2014. Vol. 617. Pp. 187-192.
 20. Timoshenko S.P., Goodier J.N. *Theory of Elasticity*, 3 Ed. McGraw-Hill, New York. 1970. 519 p.
 21. Schleicher F. Die Verteilung der Bodenpressungen unter starren Gründungskörpern" (Distribution of Soil Pressures Under Rigid Foundation Bodies). *Der Bauingenieur*. 1933. Vol. 14. Pp. 242-245.
 22. Johnson W., Mahtab F.U., Willams A. Further experiments concerning geometrically similar indentations. *Int. J. Mech. Sci.* 1966. No. 1(8). Pp. 49-59.
 23. Kitaeva D.A., Pazylov S.T., Rudaev Ya.I. Temperature-strain rate deformation conditions of aluminum alloys, *Journal of Applied Mechanics and Technical Physics*. 2016. No. 2(57). Pp. 352-358.
 24. Semenov A.S. *Vychislitel'nye metody v teorii plastichnosti* [Computational methods in theory of plasticity]. St.-Petersburg: Izd-vo SPbGPU. 2008. 211 p. (rus)
 25. [Online] URL: <http://www.mscsoftware.com/product/marc> (date of application: 07.11.2017)
- causes of cyclical instability at computations of large elasto-plastic strains // *Proc. SPIE*. 2005. Vol. 5831. Pp. 167-173.
18. Павлов П.А., Айнабеков А.И., Раимбердиев Т.П., Мельников Б.Е. Длительная прочность сталей в условиях сложного и термомеханического нагружения. Алматы: Фылым. 1996. 247 с.
 19. Melnikov B.E., Semenov A.S. Fatigue damage accumulation under the complex varying loading // *Applied Mechanics and Materials*. 2014. Vol. 617. Pp. 187-192.
 20. Тимошенко С.П., Гудьер Дж. Теория упругости. М.:Наука, 1975. 576 с.
 21. Schleicher F. Die Verteilung der Bodenpressungen unter starren Gründungskörpern (Distribution of Soil Pressures Under Rigid Foundation Bodies) // *Der Bauingenieur*. 1933. Vol. 14. Pp. 242-245.
 22. Johnson W., Mahtab F.U., Willams A. Further experiments concerning geometrically similar indentations // *Int. J. Mech. Sci.* 1966. № 1(8). Pp. 49-59.
 23. Kitaeva D.A., Pazylov S.T., Rudaev Ya.I. Temperature-strain rate deformation conditions of aluminum alloys // *Journal of Applied Mechanics and Technical Physics*. № 57(2). 2016. Pp. 352-358.
 24. Семенов А.С. Вычислительные методы в теории пластичности. СПб.: Изд-во СПбГПУ, 2008. 211 с.
 25. [Электронный ресурс] URL: <http://www.mscsoftware.com/product/marc> (дата обращения:07.11.2017)

Artem Semenov,
+7(905)2721188;
Semenov.Artem@googlemail.com

Sergey Semenov,
+7(921)9834456; ssgrus@gmail.com

Boris Melnikov,
+7(812)5526303; melnikovboris@mail.ru

Vadim Tikhonov,
+7(910)4936512;
Vadim.Tikhonov@eu.weatherford.com

Арте́м Семенович Семенов,
+7(905)2721188;
эл. почта: Semenov.Artem@googlemail.com

Сергей Георгиевич Семенов,
+7(921)9834456;
эл. почта: ssgrus@gmail.com

Борис Евгеньевич Мельников,
+7(812)5526303;
эл. почта: melnikovboris@mail.ru

Вадим Семенович Тихонов,
+7(910)4936512; эл. почта:
Vadim.Tikhonov@eu.weatherford.com

© Semenov A.S., Semenov S.S., Melnikov B.E., Tikhonov V.S., 2017